AGU ADVANCING EARTH AND SPACE SCIENCES

Earth and Space Science

RESEARCH ARTICLE
10.1029/2023EA003492

Frictional Properties of Feldspar-Chlorite Gouges and Implications for Fault Reactivation in Hydrothermal Systems

Zijuan Hu[1,2], Chongyuan Zhang[2,3,4], Lei Zhang[5], Derek Elsworth[6,7], Fengshou Zhang[8], Quan Gan[9], Huiru Lei[5], Manchao He[3], and Leihua Yao[1]

[1]School of Engineering and Technology, China University of Geosciences (Beijing), Beijing, China, [2]Institute of Geomechanics, Chinese Academy of Geological Sciences, Beijing, China, [3]School of Mechanics and Civil Engineering, China University of Mining and Technology, Beijing, China, [4]Technology Innovation Center for In-situ Stress, Ministry of Natural Resources, Beijing, China, [5]State Key Laboratory of Earthquake Dynamics, Institute of Geology, China Earthquake Administration, Beijing, China, [6]Department of Energy and Mineral Engineering, EMS Energy Institute and G3 Center, the Pennsylvania State University, State College, PA, USA, [7]Department of Geosciences, the Pennsylvania State University, University Park, PA, USA, [8]Department of Geotechnical Engineering, College of Civil Engineering, Tongji University, Shanghai, China, [9]School of Resources and Safety Engineering, Chongqing University, Chongqing, China

Key Points:

- Pure-feldspar gouge changes from velocity-strengthening to velocity-weakening with increasing temperatures
- At elevated pore pressures, pure-feldspar gouge remains slightly velocity-weakening
- Chlorite formed under feldspar chloritization reduces frictional strength but minimizes fault instability at hydrothermal conditions

Supporting Information:

Supporting Information may be found in the online version of this article.

Correspondence to:

C. Zhang,
zhchongyuan@126.com;
zhangchy@cags.ac.cn

Citation:

Hu, Z., Zhang, C., Zhang, L., Elsworth, D., Zhang, F., Gan, Q., et al. (2024). Frictional properties of feldspar-chlorite gouges and implications for fault reactivation in hydrothermal systems. *Earth and Space Science*, *11*, e2023EA003492. https://doi.org/10.1029/2023EA003492

Received 25 DEC 2023
Accepted 9 JUL 2024

Author Contributions:

Conceptualization: Chongyuan Zhang
Data curation: Zijuan Hu
Formal analysis: Chongyuan Zhang, Fengshou Zhang
Methodology: Zijuan Hu, Lei Zhang, Derek Elsworth
Validation: Zijuan Hu, Chongyuan Zhang
Writing – original draft: Zijuan Hu
Writing – review & editing: Chongyuan Zhang, Lei Zhang, Derek Elsworth, Fengshou Zhang, Quan Gan, Huiru Lei, Manchao He, Leihua Yao

Abstract

As a particularly common mineral in granites, the presence of feldspar and feldspar-chlorite gouges at hydrothermal conditions has important implications in fault strength and reactivation. We present laboratory observations of frictional strength and stability of feldspar (K-feldspar and albite) and feldspar-chlorite gouges under conditions representative of deep geothermal reservoirs to evaluate the impact on fault stability. Velocity-stepping experiments are performed at a confining stress of 95 MPa, pore pressures of 35–90 MPa, and temperatures of 120–400°C representative of in situ conditions for such reservoirs. Our experiment results indicate that the feldspar gouge exhibits strong friction ($\mu \sim 0.71$) at all experimental temperatures (~120–400°C) but when $T > 120$°C, the frictional response transitions from velocity-strengthening to slightly velocity-weakening. At constant confining pressure and temperature, increasing the pore pressure increases the friction coefficient (~0.70–0.85) and the gouge remains slightly velocity weakening. The presence of alteration-sourced chlorite leads to a transition from velocity weakening to velocity strengthening in the mixed gouge at experimental temperatures and pore pressures. As a ubiquitous mineral in reservoir rocks, feldspar is shown to potentially contribute to unstable sliding over ranges in temperature and pressure typical in deep hydrothermal reservoirs. These findings emphasize that feldspar minerals may increase the potential for injection-induced seismicity on pre-existing faults if devoid of chloritization.

Plain Language Summary

Granites are an important host for deep geothermal reservoirs where the potential hazard of injection-triggered seismicity offsets the advantages of low-carbon energy. Feldspars in these granites are susceptible to water-rock interactions and produce chlorite under appropriate hydrothermal conditions. Previous studies have shown that chlorite-rich gouges, as well as its coexistence with other minerals (not yet including feldspar), may generate aseismic sliding during fluid-injection into such reservoirs. We conduct laboratory measurements of frictional properties of simulated feldspar and feldspar-chlorite mixed gouges to determine the likelihood of generating earthquakes. We show that high temperatures and pore pressures may favor unstable sliding on feldspar gouges–and thus the potential to generate earthquakes. However, chlorite as an alteration product stabilizes faults and reduces the potential for earthquakes. We emphasize the importance of feldspar and its chloritization in modulating fault slip and the possible risk of triggered earthquakes in anthropogenic hydrothermal systems.

1. Introduction

Fluid injection triggering fault reactivation and thus induced seismicity during unconventional resource extraction such as for shale gas recovery and geothermal energy has received widespread attention (Ellsworth, 2013; Majer et al., 2007; Schultz et al., 2020). Fluid pressures in the reservoirs may increase with large-volume and high-rate injections and reactivate pre-existing natural fractures and faults, thus enhancing the potential for induced seismicity (Bao & Eaton, 2016; Eyre et al., 2019; Faulkner et al., 2018; Hubbert & Rubey, 1959; Schultz et al., 2020; Zhang, Fan, et al., 2024). Thus, understanding the mechanisms of fluid-triggered seismicity is

essential in mitigating the hazard (Hunfeld et al., 2017). Mature faults are typically gouge-filled, and gouge composition exerts control on the frictional properties (including both strength and sliding stability) and the potential for induced earthquakes (Ikari et al., 2011; Niemeijer & Spiers, 2007; Scholz, 1998, 2019). Therefore, the static and dynamic (mainly the evolution related to the sliding velocity and history of faults) frictional properties of fault gouge are significant in defining the seismic response of faults. Variations in reservoir temperature as well as fluid pressures impact frictional properties and are important to define (An et al., 2020; Andrés et al., 2019; Faulkner et al., 2018; van der Elst et al., 2013).

Both natural and simulated fault gouges have been used in previous friction experiments over a broad range of temperatures and pressures to explore the frictional stability of faults, including for granite. A characteristic of granite gouges is that strength and stability are strongly influenced by temperature–increasing temperature results in a transition from velocity weakening to velocity strengthening (Blanpied et al., 1991, 1995; Lockner et al., 1986). Specifically, the frictional properties of quartz and feldspar, the main constituent minerals in granites, have also been the subject of extensive experimental studies. Under hydrothermal conditions, quartz-rich fault gouge commonly exhibits high frictional strength ($\mu \sim 0.7$) and promote velocity-weakening behavior at ∼100−300°C, while at higher (>300°C) and lower (<100°C) temperatures the response is velocity-strengthening (Bedford et al., 2022; Chester & Higgs, 1992; Lu & He, 2018; Masuda et al., 2019). The major feldspar-group minerals in the crust are anorthite ($CaAl_2Si_2O_8$), albite ($NaAlSi_3O_8$) and K-feldspar ($KAlSi_3O_8$). Among them, the anorthite-albite series (plagioclase) are the most abundant minerals. To date, few experiments define the frictional properties of feldspar under hydrothermal conditions typical of the shallow crust–representative of triggering effect of deep geothermal energy recovery. A few experimental studies define the frictional strength of plagioclase as similar to quartz, with a coefficient of friction of ∼0.7 (Masuda, 2020; Masuda et al., 2019). However, compared with quartz, plagioclase tends to remain velocity weakening at higher temperatures. Over the temperature range 200–500°C, plagioclase is velocity weakening with negative ($a-b$) values (He et al., 2013; Masuda, 2020; Masuda et al., 2019) suggesting the potential for seismic reactivation.

In addition to the comminution products from granites, as quartz and feldspar, metamorphic transformations under long-term hydrothermal conditions produce important alteration products–again with potentially key controls on frictional stability (Brown et al., 2003; Okamoto et al., 2019). For example, chlorite is a widespread product of hydrothermal alteration within subducting oceanic crust and geothermal reservoirs (Elders et al., 1979; Morrow et al., 2000; Okamoto et al., 2019; Schiffman & Fridleifsson, 1991), generally resulting from the alteration or as products of water-rock interactions (Lucie, 2016; Yuguchi et al., 2015, 2021). Under hydrothermal conditions, chlorite is produced on many pathways, one of which is the dissolution of feldspar in the presence of weakly alkaline pore fluids in the temperature range ∼210–350°C (Yuguchi et al., 2021), representative of deep geothermal reservoirs. Previous laboratory studies of simulated chlorite-rich gouges sheared at elevated temperatures and pore pressures indicate relatively low shear strengths (frictional coefficient $\mu < 0.5$) although velocity strengthening behavior (An et al., 2021; Fagereng & Ikari, 2020; Ikari et al., 2009; Okamoto et al., 2019; Shimamoto & Logan, 1981). Under hydraulic stimulation in enhanced geothermal systems (EGS) reservoirs, feldspar chloritization as one of the sources of chlorite has the potential to evolve over engineering timescales and in fracture systems newly accessed in geothermal reservoirs. Therefore, a careful understanding of the frictional properties of feldspar chloritization is important in evaluating and ameliorating potential injection-triggered seismic risks.

Typical geological hosts for deep geothermal reservoirs are granitic and with abundant low-grade metamorphic minerals (such as laumontite, chlorite and epidote) developed with in the reservoirs (An et al., 2021; Okamoto et al., 2019; Zhang, Hu, et al., 2024). In addition, typical EGS reservoirs often host pyrite, indicative as a geothermometer of hydrothermal intrusion >250°C (Zhang, Huang, et al., 2022; Zhang, Wen, et al., 2022)–with 250°C present within the stability field for chlorite. In addition, feldspar is hydrolyzed in a weakly alkaline environment at this temperature and with the potential to form chlorite (Yuguchi et al., 2021). Such feldspar-chloritization can be found in the Matouying EGS reservoir of North China (Zhao et al., 2020; Figure 1). To constrain the impact of feldspar gouge and such chloritization pathways on the stability of faults in such generic granitic reservoirs, we conduct friction-stability experiments on feldspar (K-feldspar and albite) and feldspar-chlorite mixtures at elevated temperatures and pore pressures typifying geothermal reservoirs.

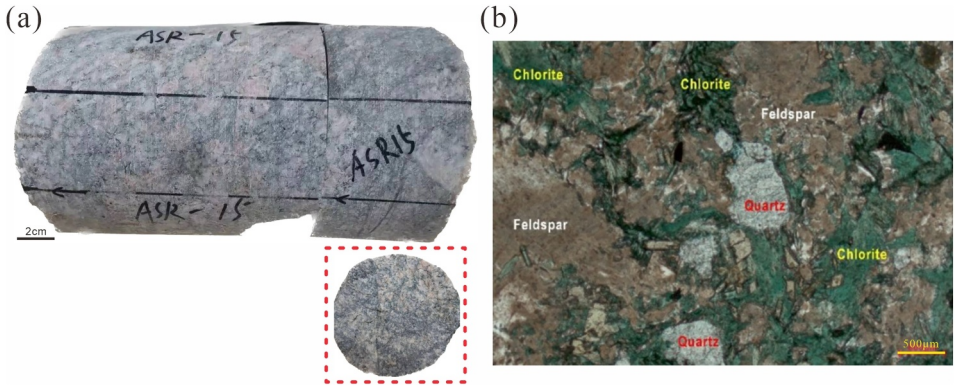

Figure 1. Photographs of (a) granite core recovered from ~3.8 km depth of the Matouying EGS reservoir in Tangshan, North China, and (b) photomicrograph showing feldspar chloritization.

2. Experimental Methods

We complete friction stability measurements on feldspar and synthetic mixed feldspar-chlorite gouges. Experiments are conducted under recreated hydrothermal conditions representative of deep geothermal systems to examine the influence of temperature and pore pressures on friction and stability.

2.1. Gouge Preparation

The feldspar and chlorite minerals used to simulate fault gouges in our experiments were obtained commercially. The mineral compositions of the two mineral powders were analyzed by X-ray diffraction (XRD) and shown to be of >99 wt.% (feldspar) and 97 wt.% (chlorite) purity (Figure 2). The mineral composition of feldspar is 53% K-feldspar and 47% albite. To simulate fault gouge, both mineral powders were crushed and sieved to pass through a #200-mesh sieve. Median particle sizes of the feldspar (18.7 μm) and chlorite (66.9 μm) (Figure 3) are defined by laser classifier. Synthetic aggregates were then prepared using feldspar and chlorite in the same proportions by weight.

2.2. Apparatus and Experimental Procedure

Shear experiments were performed using a triaxial testing apparatus with argon as the confining gas and located at the Institute of Geology, China Earthquake Administration, Beijing, China. A schematic of the sample assembly is shown in Figure 4 (He et al., 2006, 2013). An electro-hydraulic servo-controlled system drives the axial displacement in the experimental apparatus, with the maximum temperature, fluid pressure, and confining pressure of 600°C, 200 MPa, and 420 MPa, respectively. Its minimum axial displacement rate reaches 10^{-2} μm/s. We add deionized water to the mineral powders and bring them to chemical equilibrium by stirring for ~10 min. Between the gabbro driving blocks with a diameter of 20 mm and a height of 40 mm

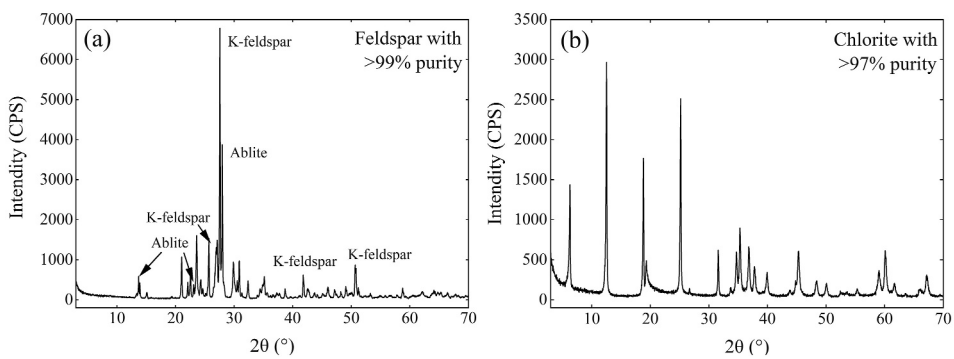

Figure 2. XRD results of feldspar and chlorite mineral powders used in the simulated fault gouges for the experiments. (a) Feldspar purity at >99 wt.% and (b) chlorite purity at >97 wt.%.

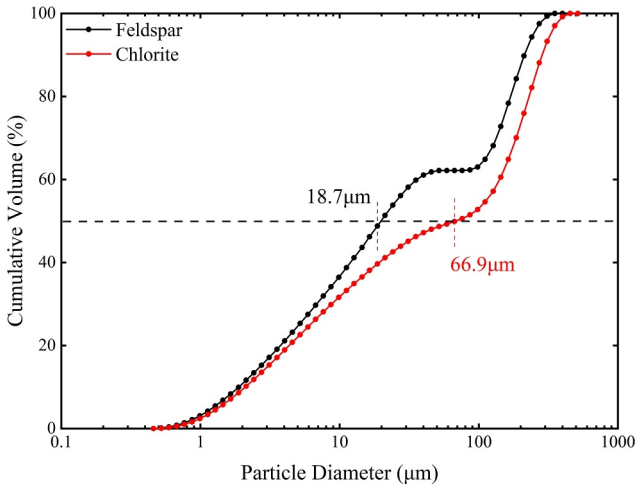

Figure 3. Particle size distributions of feldspar and chlorite gouges for the friction-stability experiments. The median particle sizes of the feldspar and chlorite gouges are 18.7 and 66.9 μm, respectively.

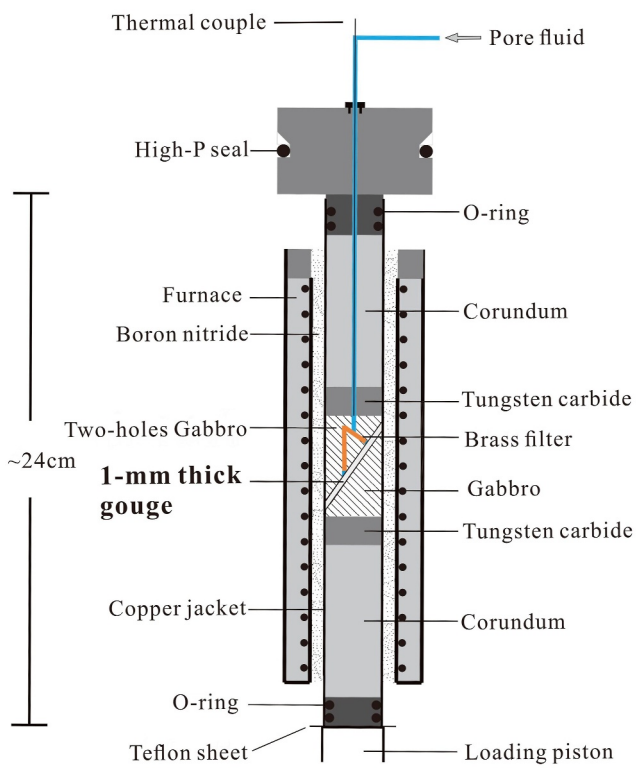

Figure 4. Schematic of the high-temperature and -pressure triaxial test apparatus. Both ends of the copper jacket are sealed with O-rings to prevent argon gas from penetrating into the fault gouge sample. A high-pressure seal on the upper piston was used to prevent the leakage of the argon gas and retain the seal on the entire assembly. A comparative test shows that using granite or gabbro as the driving blocks will have no significant effect on the experimental results (Figure S2 in Supporting Information S1).

sandwiched a 1-mm-thick gouge layer. The sawcut surface of the driving blocks is inclined at 35° to the loading axis. The sawn surfaces of the simulated fracture zones of the upper and lower drive blocks are roughened with a 200-mesh silicon carbide polishing compound. The upper driving block was drilled with two interconnected 2-mm-microboreholes providing fluid access to the gouge layer, and thus access to pore pressures. A brass filter was placed within the holes to prevent gouge extrusion. The assembled gouge and gabbro driving blocks were held in place by a precise hollow cylindrical fixture, which can assist in placing the driving blocks sandwiching the gouge into the copper jacket. Then, we placed the assembled sample in an annealed copper sleeve with 0.35-mm thickness. Both ends of the assembled sample are sealed with double O-rings seal to prevent argon gas from intruding into the gouge layer. A thermocouple monitors the temperature fluctuations close to the fault gouge and an independent controller was applied to maintain temperature fluctuations constant within ±1°C throughout experiments. We increase the confining pressure (argon gas) to initiate each experiment, then inject water to increase the pore pressure to 2/3 of the target pressure, heat to the target temperature and then fully pressurize to the desired value. Fluctuations of confining and pore pressures were maintained constant within ±0.3 and ±0.1 MPa through two servo-controlled boosters, respectively. All stress and displacement data were recorded at a sampling frequency of 1 Hz, except for a sampling frequency of 10 Hz at the maximum loading rate.

We conducted a total of 14 shear experiments for monomineralic gouges (feldspar) and uniformly mixed feldspar-chlorite gouges (1:1) at constant confining pressure (P_c = 95 MPa), different temperatures (T = 120, 180, 300, and 400°C) and different pore pressures (P_f = 35, 50, 70 and 90 MPa) representing conditions relevant to the depth of fluid injection for the 3.7 km Gonghe geothermal reservoir in northeastern Tibetan Plateau, China. Details are shown in Table 1. The results are representative of EGS development with the pore pressure P_f = 35 MPa and confining pressure P_c = 95 MPa representing the hydrostatic and lithostatic pressure at ~3.7-km depth (assuming a rock density of 2,630 kg/m^3) in the EGS reservoir at Gonghe site. In addition, the elevated pore pressures P_f = 50–90 MPa are consistent with fluid injection during reservoir stimulation. In the initial stage of the velocity stepping experiments, the gouge was sheared at a constant axial loading velocity of 0.5 μm/s until steady-state friction was achieved. Then, the axial loading velocity was stepped between 5, 0.5 and 0.05 μm/s, corresponding to shear velocities of 6.1, 0.61 and 0.061 μm/s, to explore the frictional properties of the feldspar and mixed feldspar-chlorite gouges.

2.3. Data Analysis

The raw data of shear experiments requires a correction due to the shear resistance from the copper jacket and the decrease in gouge contact area with shearing (Text S1 in Supporting Information S1). The shear (τ) and normal stresses (σ_n) were obtained with processing the corrected data. Friction coefficient of the synthetic gouge μ is

$$\mu = \frac{\tau}{\sigma_{neff}} = \frac{\tau}{(\sigma_n - P_f)} \quad (1)$$

where the σ_{neff} is the effective normal stress and P_f is the pore pressure.

Table 1
Experimental Matrix and Key Data

Testing ID	Gouge	T (°C)	P_c (MPa)	P_f (MPa)	σ_{neff} (MPa)	l_{final} (mm)
Data set 1: Pure gouge at constant P_c = 95 MPa						
CK-08	Fsp	120	95	35	118	3.49
CK-07	Fsp	180	95	35	117	3.71
CK-12	Fsp	180	95	50	89	4.04
CK-14	Fsp	180	95	70	52	3.53
CK-10	Fsp	180	95	90	13	3.20
CK-06	Fsp	300	95	35	120	3.32
CK-05	Fsp	400	95	35	120	3.64
Data set 2: Mixed gouges at constant P_c = 95 MPa						
CK-09	50% Fsp + 50% Chl	120	95	35	95	3.83
CK-01	50% Fsp + 50% Chl	180	95	35	96	2.28
CK-11	50% Fsp + 50% Chl	180	95	50	74	3.58
CK-13	50% Fsp + 50% Chl	180	95	70	43	3.14
CK-02	50% Fsp + 50% Chl	180	95	90	10	3.36
CK-04	50% Fsp + 50% Chl	300	95	35	95	2.93
CK-03	50%Fsp + 50% Chl	400	95	35	105	2.86

Note. Fsp = Feldspar, Chl = Chlorite, P_c = confining pressure, P_f = pore pressure, σ_{neff} = effective normal stress, T = temperature, l_{final} = final shearing displacement. Note that the effective normal stress is obtained from $\sigma_{neff}=(P_c-P_f)/(1-\mu\cot\beta)$, where β is the fault angle (He et al., 2013).

Based on the theory of rate- and -state-friction (RSF), the velocity dependence parameter ($a-b$) was estimated (Dieterich, 1978; Ruina, 1983; Scholz, 1998). For RSF friction, the friction coefficient μ is expressed as

$$\mu = \mu^* + a\ln\left(\frac{V}{V^*}\right) + b\ln\left(\frac{V^*\theta}{D_c}\right) \tag{2}$$

$$\frac{d\theta}{dt} = 1 - \frac{V\theta}{D_c} \tag{3}$$

where μ^* is the frictional coefficient at the reference shear velocity V^*, a is the friction parameter reflecting the direct effect, b is the evolution effect of the shear velocity transition and Dc denotes the critical slip distance at which frictional strength evolves to a new steady state as the state variable θ approaches unity.

At a steady friction state, the state variable θ does not change with time t and thus $d\theta/dt = 0$. Then, combining Equations 2 and 3, yields the velocity dependence parameter (a–b) as

$$a - b = \frac{\mu - \mu^*}{\ln(V/V^*)} \tag{4}$$

Negative values of ($a-b$) indicate that frictional coefficient decreases with increasing velocity, namely, velocity weakening behavior. Fault gouges with negative ($a-b$) may host unstable fault slip if the fault system stiffness falls below the critical stiffness. Thus, velocity-weakening behavior provides the potential for stick-slip and may result in earthquake nucleation (Marone, 1998; Scholz, 1998). Conversely, velocity-strengthening behavior is indicated with positive values of ($a-b$) and promote inherently stable sliding and inhibit seismic rupture. The values of ($a-b$) under stable sliding can be recovered directly from the friction–displacement curves (Figures S1a and S1b in Supporting Information S1). Conversely, the values of ($a-b$) for quasi-static oscillations or stick-slip may be obtained from data fitting (Figure S1c in Supporting Information S1, more details in He et al., 2013), as completed here.

The potential for induced earthquakes requires that velocity-weakening conditions and a fault stiffness below the critical stiffness (K_{cr}) are both met. Fault instability results when $(a–b) < 0$ and the critical stiffness K_{cr} is larger than the loading stiffness K, that is, $K_{cr} \geq K$ (Gu et al., 1984). The critical stiffness of the fault (He et al., 2013; Ruina, 1983) is defined as

$$K_{cr} = \frac{-(a-b)\cdot\sigma_{neff}}{D_c} \tag{5}$$

where D_c is the characteristic slip distance and σ_{neff} is the effective normal stress. Due to the necessary condition of velocity weakening for the unstable sliding of faults, $(a–b)$ is a topical parameter in shear experiments. Thus, we use the values of $(a–b)$ as indices to explore the sliding behavior of faults in our study.

2.4. Microstructural Methods

Post-shear, we carefully removed the forcing blocks (corundum and tungsten carbide) retaining only the gabbro driving blocks and gouge in the copper jacket. The samples were then placed into rubber molds and vacuum-impregnated with epoxy resin before being cured in an oven at 65°C for ∼24 hr. Once completely hardened, thin sections were then prepared by slicing along the shear (axial loading) direction. The thin sections were then polished and sprayed with gold on the surface. Microstructures were examined using scanning electron microscopy (SEM).

3. Results

We report experiments on both pure-feldspar and felspar-chlorite gouges to examine the impact of feldspar and feldspar chloritization of friction and frictional stability, and link response to microstructural observations. The detailed friction-displacement data of each experiment are stored in a database (Hu et al., 2023).

3.1. Feldspar Gouge

Our friction-displacement experimental curves for the feldspar initially exhibit a linear increase in friction (shear stress to normal stress ratio) with displacement followed by inelastic yield point then steady state friction at a shearing displacement of ∼1.83 mm (Figure 5). Subsequently, a weak strain hardening response develops until a final shear displacement of 3–4 mm (Table 1 and Figure 5). The simulated feldspar gouge shows stable sliding at T = 120°C and P_f = 35 MPa (Figure 5a), while stick-slips were observed at a shear velocity of 0.061 μm/s at T = 180°C (Figure 5b). As shown in Figure 4, the feldspar gouge exhibits a stable sliding at $T >$ 180°C. A small oscillation lasting for ∼0.1 mm of displacement occurs when the shear rate is switched to 6.1 μm/s at T = 300°C (Figure 5f). The friction-displacement curves of the feldspar fault gouge show stable sliding and a strong dependence of friction coefficient on velocity (Figure 5g). Notably, we observe a slip weakening trend for feldspar gouge at T = 180°C and P_f = 90 MPa (Figure 5e). The coefficient of friction μ of feldspar gouge is characterized by a distinct peak at a shear displacement of ∼0.6 mm and then a decay to a steady state value with increasing shear displacement (Figure 5e). This phenomenon is possibly explanted by the shear strength of fault gouge being significantly impacted by its cohesive strength at low effective pressure, that is, it is possible that low effective stress causes slip weakening at P_f = 90 MPa. The frictional coefficient at steady state was measured at a shear displacement of ∼1.83 mm for each experiment (except for P_f = 90 MPa where at ∼3 mm). Our results indicate that the frictional coefficient of feldspar gouge is ∼0.71 over the range of experimental temperature (120–400°C), with no significant change with increasing temperature (Figure 7a). In contrast, the frictional coefficient μ for the simulated feldspar gouge at different pore pressures are in the range ∼0.70–0.85 and increase with pore pressure (Figure 7b).

The frictional stability $(a–b)$ for the simulated feldspar gouge was calculated based on the methods in Section 2.3 with the results shown in Table 2. A transition from velocity strengthening behavior to slightly velocity weakening behavior can be identified at T = 120–180°C and P_f = 35 MPa. This is then followed by a transition to velocity strengthening at T = 300°C and finally to slightly velocity weakening at T = 400°C. This indicates that, temperature has a significant impact on stability of the feldspar gouge (Figure 7c and Figure S3a in Supporting Information S1). At T = 180°C and P_f = 35–90 MPa, the feldspar gouge exhibits slightly velocity-weakening behavior (Figure 7d and Figure S3b in Supporting Information S1). Moreover, the effective normal stress also

10.1029/2023EA003492

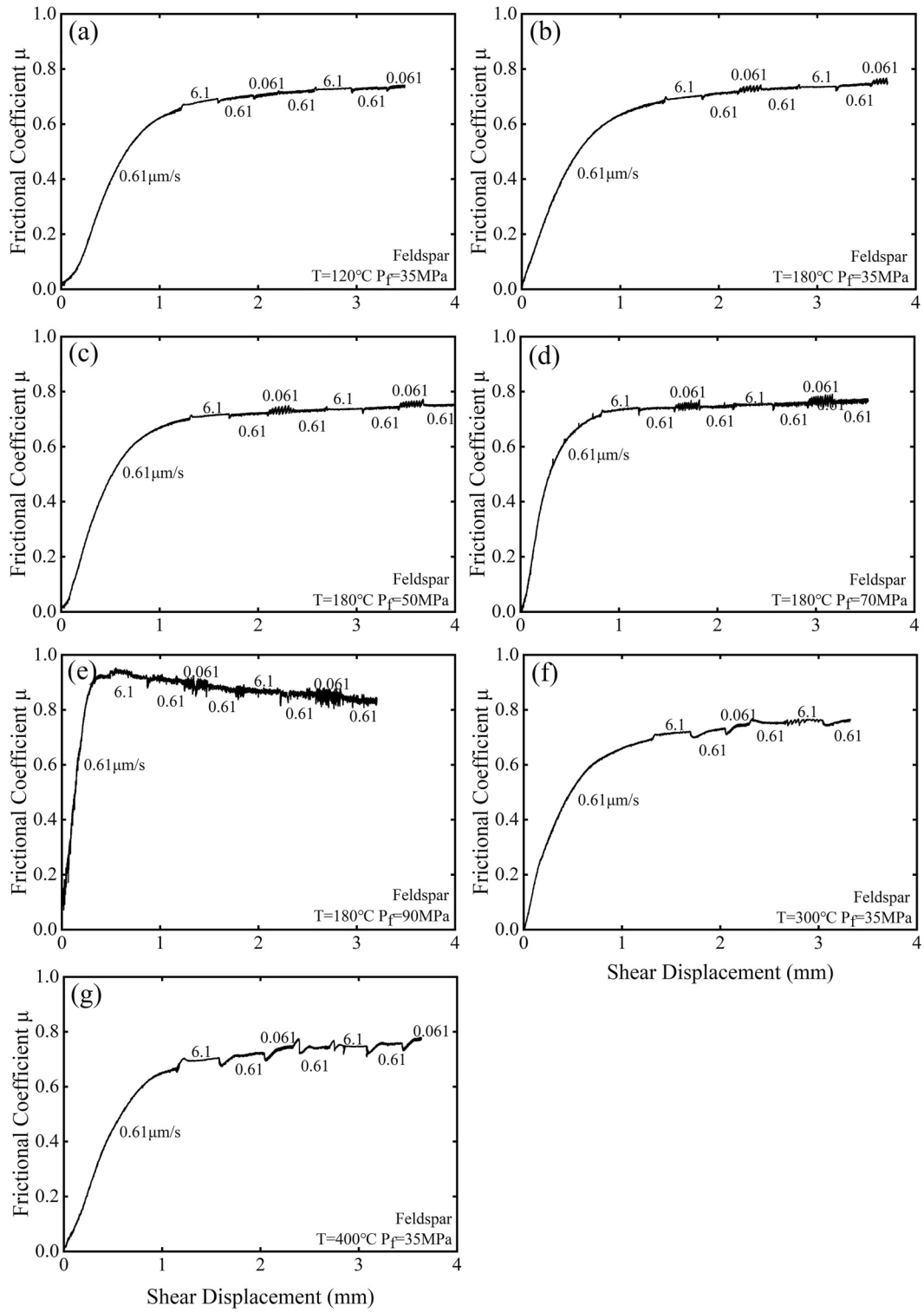

Figure 5. Friction-displacement curves for the feldspar gouge. The feldspar gouge shows a slightly velocity-weakening trend at T = 180°C, 400°C and P_f = 35–90 MPa.

significantly affects the velocity dependence of frictional stability. At T = 180°C, a higher effective normal stress returns a more negative value of ($a-b$) that increases with increasing effective normal stresses (Figure 7e and Figure S3c in Supporting Information S1). In summary, higher effective normal stresses promote velocity-

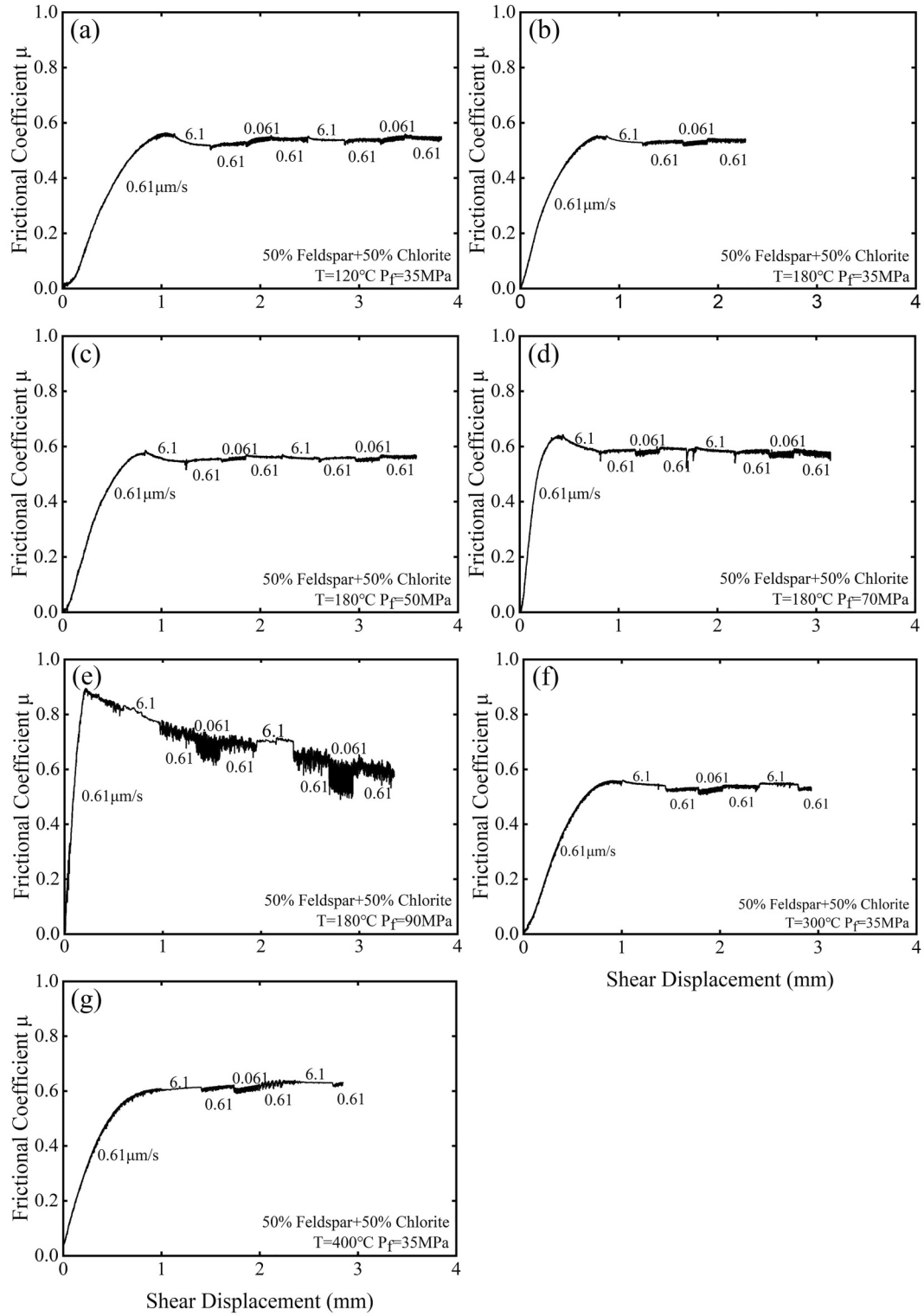

Figure 6. Friction-displacement curves for the feldspar-chlorite mixed gouges. The mixed gouges exhibit velocity-weakening behavior only at $T = 120$°C.

weakening behavior at constant temperature. In addition, we analyzed the variation of friction stability with shear velocity–the feldspar gouge exhibits a relatively apparent velocity-weakening behavior at lower shear velocities in the range of the experimental temperatures ($T = 180$–400°C) and pressures (Figures 8a and 8b).

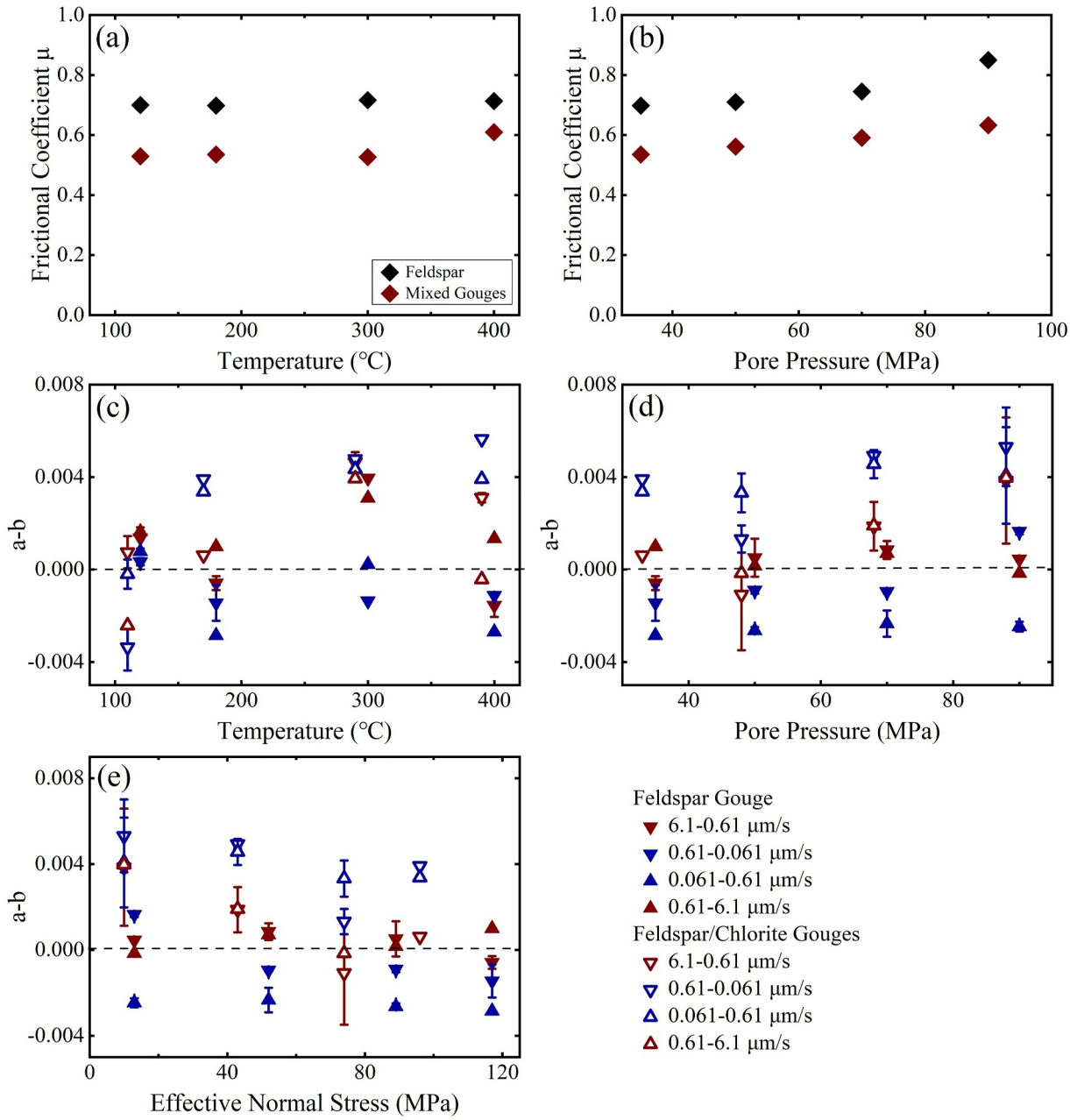

Figure 7. Frictional coefficient μ and frictional stability ($a-b$) for feldspar and feldspar-chlorite mixed gouges at different temperatures and pressures. (a) Magnitudes of μ versus temperature of pure feldspar gouge and mixtures at $P_c = 95$ MPa and $P_f = 35$ MPa. (b) Relationship between friction coefficient and pore pressure of pure gouge and mixtures at $T = 180$°C. (c) ($a-b$) as a function of temperatures for pure feldspar gouge and mixtures at $P_f = 35$ MPa. (d) ($a-b$) as a function of pore pressure of pure gouge and mixtures at $T = 180$°C. (e) ($a-b$) as a function of effective normal stress of pure gouge and mixtures at $T = 180$°C. Note that μ_{ss} is the steady state value of frictional coefficient at a shear displacement of ~1.83 mm (~3 mm at $P_f = 90$ MPa) and a shear velocity of 0.61 μm/s. The plotted ($a-b$) values are the average values from the same velocity steps in each test with the error calculated from the standard deviation.

3.2. Mixed Feldspar-Chlorite Gouges

We evaluate the competing influences of feldspar and the alteration mineral chlorite on the frictional stability of the gouge. After ~1.83 mm of shear displacement (except at ~3 mm for $P_f = 90$ MPa), the friction–displacement curves exhibit a slight strain strengthening and stable sliding to a final shear displacement of 3–4 mm (Figure 6). The mixed gouges slide stably over the range of experimental temperatures $T = 120$–300°C (Figures 6a and 6f).

Table 2
Frictional Coefficient μ and Velocity Dependence Parameter (a−b) at Each Velocity Step of the Shear Experiments

		$a-b$ values at (μm/s)						
Test ID	μ_{ss}	F6.1-0.61	F0.61-0.061	F0.061-0.61	F0.61-6.1	S6.1-0.61	S0.61-0.061	S0.061-0.61
CK-08	0.6998	0.00104	0.00023	0.00078	0.00163	0.00169	0.00045	–
CK-07	0.698	−0.00080	−0.00200	−0.00285	0.00099	−0.00038	−0.00090	–
CK-12	0.71	0.00109	−0.00100	−0.00274	0.00016	−0.00008	−0.00080	−0.00253
CK-14	0.7451	0.00112	−0.00090	−0.00274	0.00070	0.00057	−0.00100	−0.00193
CK-10	0.8498	0.00047	0.00174	−0.00232	−0.00016	0.00043	0.00156	−0.00261
CK-06	0.7161	0.00395	−0.00136	0.00022	0.00309	–	–	–
CK-05	0.7132	−0.00117	−0.00115	−0.00270	0.00134	−0.00193	−0.00108	–
CK-09	0.5291	0.00124	−0.00407	−0.00064	−0.00242	0.00026	−0.00264	0.00025
CK-01	0.5352	0.00062	0.00391	0.00337	–	–	–	–
CK-11	0.5616	−0.00278	0.00090	0.00272	−0.00016	0.00063	0.00174	0.00391
CK-13	0.5909	0.00261	0.00478	0.00413	0.00190	0.00113	0.00507	0.00499
CK-02	0.6323	0.00192	0.00411	0.00259	0.00397	0.00578	0.00651	0.00554
CK-04	0.5264	0.00434	0.00478	0.00434	0.00394	0.00495	–	–
CK-03	0.6094	0.00294	0.00565	0.00391	−0.00043	0.00328	–	–

Note. As most of our shear experiments were conducted for identical velocity step sequences of "0.61-6.1-0.61-0.061--0.61-6.1-0.61-0.061-0.61 μm/s," the first (F) and second (S) velocity steps indicate the same magnitude of velocity change but at different shear displacements. The first velocity step (0.61–6.1 μm/s) was not representative of the steady state and was excluded from our calculations. The values of (a–b) are averaged identical velocity steps in each experiment and the error calculated from the standard deviation are also shown in Table S1 in Supporting Information S1. μ_{ss} is the frictional coefficient determined at shear displacement of ∼1.83 mm but at ∼3 mm for $P_f = 90$ MPa, due to the effective stress being too low and resulting in reaching the residual friction value only at that shear displacement of ∼3 mm.

At $T = 400$°C and for a shearing rate $V = 0.61$ μm/s, small oscillation in friction result, lasting ∼0.2 mm, followed by stable sliding (Figure 6g). The results show that the mean frictional coefficient for the mixed gouges is ∼0.55, with the coefficient of friction μ at $T = 400$°C deviating significantly from that at $T \leq 300$°C (Figure 7a). The frictional strength increases with increasing pore pressure and as expected the friction coefficient is less than that for the feldspar gouge (Figure 7b).

Trends in frictional stability (a–b) at the given temperature and pore pressure for the feldspar-chlorite mixed gouges are illustrated in Figure 7 and Table 2. This sample exhibits a transition from velocity weakening at $T = 120$°C and $P_f = 35$ MPa (a–$b = -0.00176$) to slight velocity strengthening at $T \geq 180$°C (a–$b = 0.00263$ to 0.00443). Frictional stability ($a-b$) increases with increasing temperature when the displacement rates were stepped between 0.61 and 0.061 μm/s. Moreover, the value of ($a-b$) shows a variety of trends as the shearing rates were stepped between 0.61 and 6.1 μm/s (Figure 8). We compared velocity dependence for both the feldspar and mixed gouges, with the mixed gouges exhibiting more velocity-strengthening at $T \geq 180$°C (Figure 7c). The friction and stability of mixed gouges vary little with pore pressure at $T = 180$°C and $P_f = 35$–50 MPa–however, ($a-b$) values increase with increasing pore pressure at $P_f \geq 50$ MPa. The frictional properties of the uniformly mixed gouges are significantly different from those of feldspar alone and shows a different trend with increasing pore pressure from that of feldspar gouge (Figure 7d). The velocity dependence parameter ($a-b$) of the mixed gouges first decreases and then increases with an increase in effective normal stress, with 74 MPa as the transition stress (Figure 7e). The values of ($a-b$) decreases with increasing effective normal stress (σ_{neff}) at $T = 180$°C and $\sigma_{neff} < 74$ MPa. This can be interpreted as the lower-bound effective stress promoting velocity-strengthening behavior of the mixed fault gouge at constant temperature. Moreover, the sliding rate influences the frictional stability of the mixed gouges. The mixed feldspar-chlorite gouges exhibit velocity-strengthening behavior within the range of experimental temperature and pressures, and ($a-b$) decreases with an increase in post step velocities at 0.61 and 6.1 μm/s (Figures 8c and 8d).

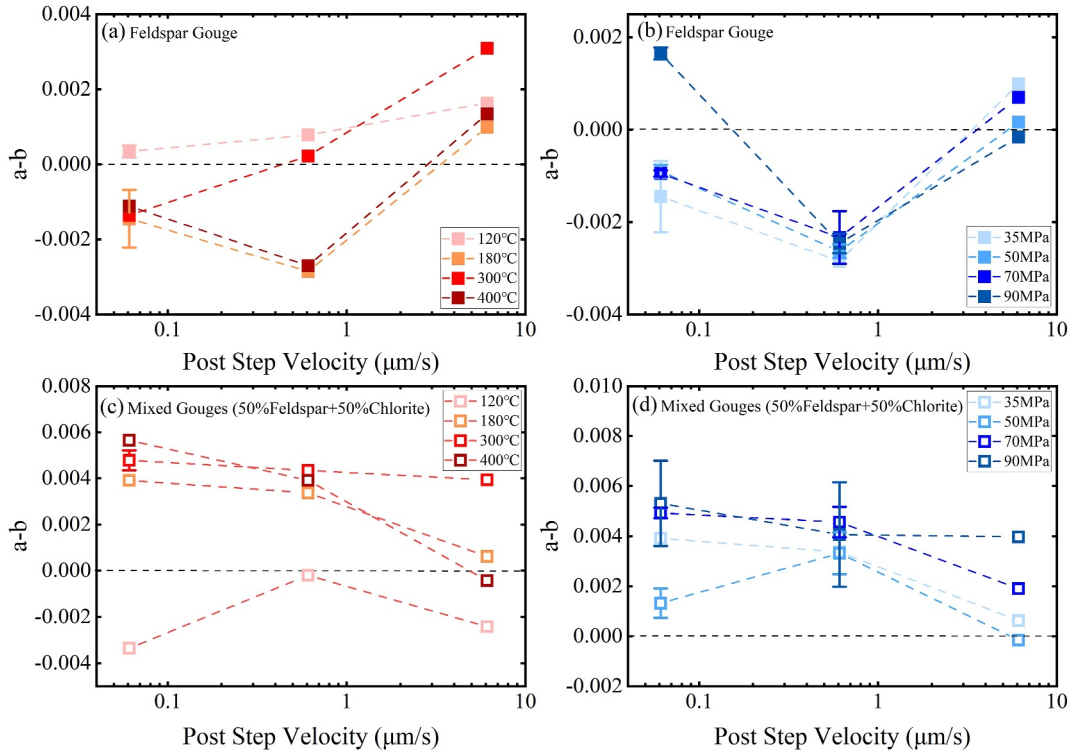

Figure 8. Frictional stability parameter (a–b) for the feldspar and feldspar/chlorite mixed gouges at various post step velocities. (a) ($a-b$) for pure feldspar gouge at P_c = 95 MPa and P_f = 35 MPa. (b) ($a-b$) for pure feldspar gouge at P_c = 95 MPa and T = 180°C. (c) ($a-b$) for feldspar-chlorite mixed gouges at P_c = 95 MPa and P_f = 35 MPa. (d) ($a-b$) for feldspar-chlorite mixed gouges at P_c = 95 MPa and T = 180°C.

3.3. Microstructural Observations

Following the method described in Section 2.4, we used SEM for microstructural observations on the deformed samples, with the methods of Logan et al. (1992) adopted to define the resulting fabric. Among, the post-experiment samples, disassembly destroyed the feldspar samples at P_f = 50 and 70 MPa and the mixed gouges at P_f = 70 MPa and T = 300°C–resulting in missing microstructures of these samples. The microstructures of the deformed gouges are illustrated in Figures 9–12. At P_f = 35 MPa and T = 120–400°C, *R1* angle shears commonly develop in the feldspar gouge (Figure 9), which varies slightly with increasing temperature. At T = 180°C, several narrow-localized shear zones develop with significant local grain crushing. Tortuous cracks penetrate throughout the fault zone (Figures 9b and 9e). When the temperature is increased to 400°C, the tortuosity of the shear cracks is more apparent than at 180°C (Figure 9e). At P_f = 35 MPa, comparative analysis of the particle size near the shear zone shows that the particles at T = 180°C and 400°C are significantly smaller than those at T = 120°C and 300°C (Figure 11). At T = 180°C, compared to inhomogeneous shear with particle sizes ranging from a few micrometers to tens of micrometers at P_f = 35 MPa, distributed shear evolve with less grain size reduction and relatively uniform particle crushing (~10−20 μm) for the deformed feldspar gouges at 90 MPa (i.e., at low effective stresses), and no obvious *R1* shear zone penetrates the fault gouge layer (Figures 9b and 9c and 11b and 11c).

For our samples of mixed gouges, the feldspar particles are surrounded by structured layers of chlorite particles (Figure 12), which is consistent with previous studies related to the microstructure of chlorite (An et al., 2021; Fagereng & Ikari, 2020; Okamoto et al., 2020). At P_f = 35 MPa and T = 180–400°C, the mixed gouge layer exhibits multiple cross-distributed groups of *R*1 shears with indistinct *R*1 shear at T = 120°C (Figure 10). Furthermore, the layered structure of chlorite particles in the mixed gouges exhibits obvious bending deformation after shearing at T = 120°C, and the degree of bending decreases with increasing temperature until almost straight layered structure occurs at T = 400°C (Figure 12). The corresponding microstructural change for the mixed gouges can be observed with elevated pore pressure. That is, a few parallel *R1* shears develop in the fault zone at

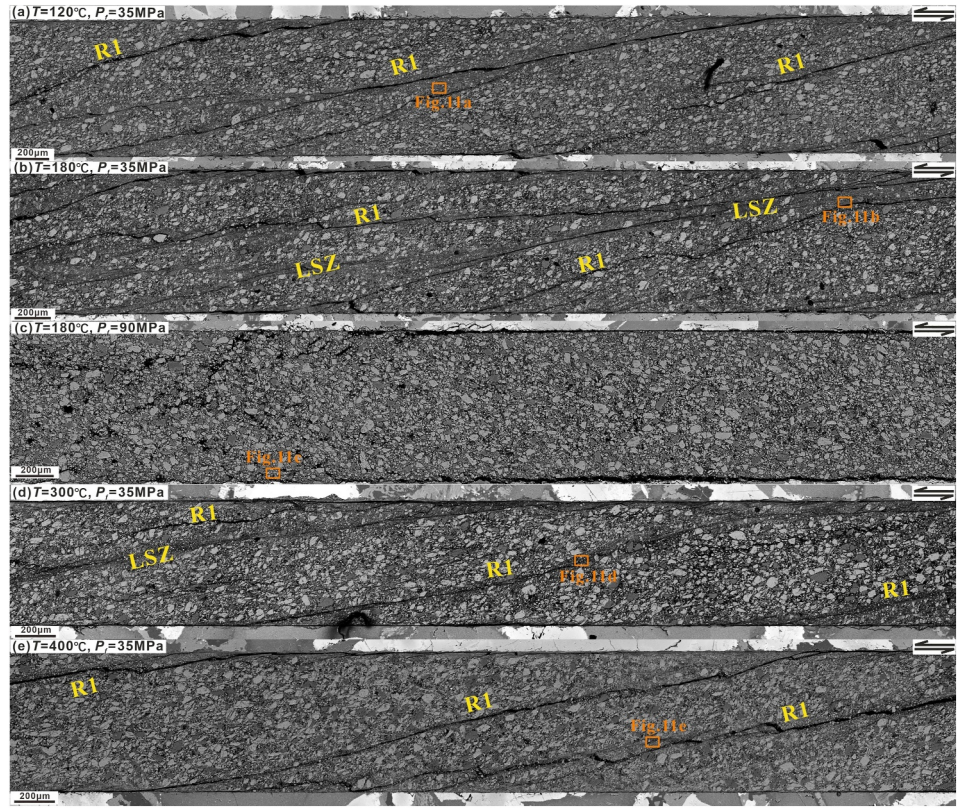

Figure 9. Microstructure (backscattered images) of the deformed feldspar gouge post-experiment. Refer to Logan et al. (1992) for relevant terms used to describe microscopic features. We observed local shear zones (LSZ) and *R1* shear (Riedel shear) in partial samples.

$P_f = 50$ MPa (Figure 10c)–however, at $P_f = 90$ MPa, the gouges can be characterized by grain fragmentation, with no obvious *R1* shear or zones of shear localization and with mineral particle sizes ranging from several micrometers to tens of micrometers (Figures 10d and 12d).

4. Discussion

We explore impacts and mechanisms of temperature and pore pressure on both pure-feldspar (Section 4.1) and mixed feldspar-chlorite gouges (Section 4.2) in controlling friction and frictional stability. We use these observations and projected mechanisms to discuss implications for injection-induced seismicity (Section 4.3) in hydrothermal systems.

4.1. Feldspar Sliding Dependence on Temperature and Pore Pressure

Previous studies suggested that both the temperatures and pore pressures are important factors influencing fault instability (Blanpied et al., 1995). Frictional strength of the feldspar gouge is insensitive to temperature in our experiments. The average value of frictional coefficient for the feldspar gouge is ~0.7, broadly consistent with previous experimental studies (He et al., 2013; Masuda, 2020; Masuda et al., 2019). At $P_f = 35$ MPa and $T = 120$–400°C, the feldspar gouge exhibits velocity-strengthening behavior at $T = 120$°C and 300°C and slightly velocity-weakening behavior at $T = 180$°C and 400°C (Figure 7c). The shear localization within gouge layers is important for promoting unstable sliding behavior to occur (Bedford & Faulkner, 2021). We observe apparent localized shear zones at moderate temperature (T = 180°C) where the sliding behavior transitions—as noted in the microstructural observations. The transition from velocity-strengthening to velocity-weakening in our shear experiments can commonly be explained by a microphysical model (Niemeijer & Spiers, 2007; den Hartog et al., 2012; Chen et al., 2015; Chen & Spiers, 2016). The model assumes that the strength and velocity dependence of the gouge is regulated by the competition between an expansion velocity (due to activated

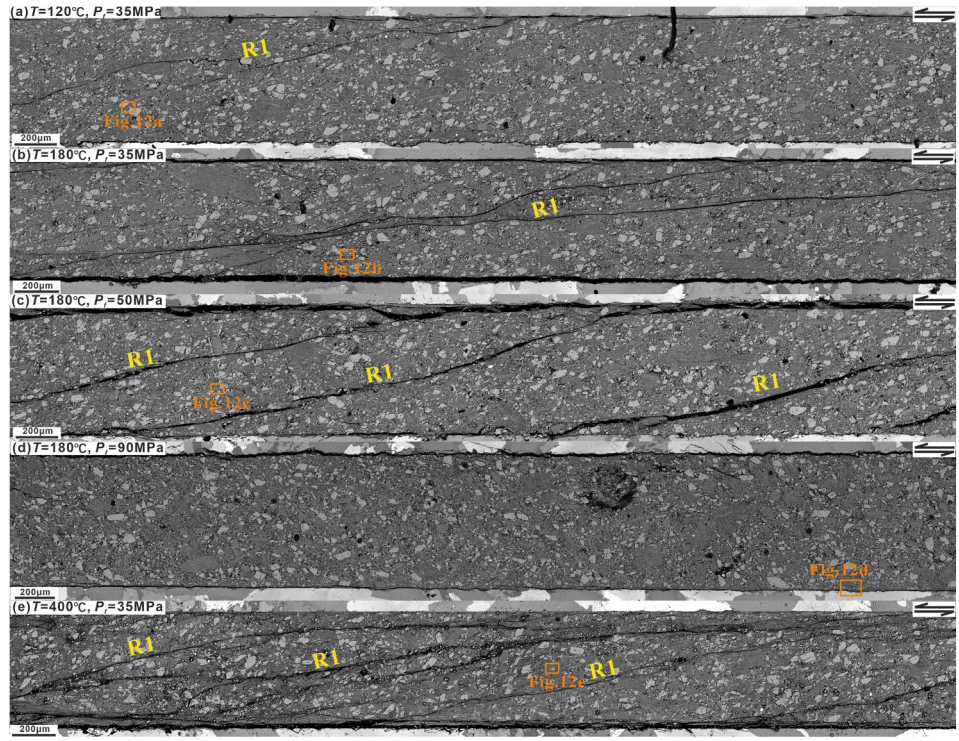

Figure 10. Microstructure (backscattered images) of the deformed feldspar-chlorite mixed gouges post-experiment. Refer to Logan et al. (1992) for relevant terms used to describe microscopic features. Experimental conditions: (a) $T = 120$°C, $P_f = 35$ MPa, (b) $T = 180$°C, $P_f = 35$ MPa, (c) $T = 180$°C, $P_f = 50$ MPa, (d) $T = 180$°C, $P_f = 90$ MPa, (e) $T = 400$°C, $P_f = 35$ MPa.

subcritical crack propagation or intergranular particle flow) and a compaction velocity (due to thermally activated pressure solution). The velocity of pressure solution increases with an increase in temperature and the gouge is further compacted. When the compaction velocity of the gouge particles is approximately equal to the expansion velocity then velocity-weakening behavior results (Chen et al., 2020; Verberne et al., 2020). Unfortunately, we did not observe remarkable features indicating pressure solution for our range of experimental temperatures, but previous experimental studies have indeed indicated the presence of intergranular pressure solution in feldspar minerals at higher temperatures (He et al., 2013). Thus, our experimental results are theoretically consistent with such a model but the link remains speculative. However, our experimental results show a velocity-strengthening behavior at $T = 300$°C which transforms to velocity weakening at $T = 400$°C (Figure 7c), which is inconsistent with the above microphysical model. This is potentially explained by processes driven by the unique properties of supercritical water ($T = 374$°C, $P_f = 22.1$ MPa; Maxim et al., 2021). We note that our experimental conditions of $T = 300$°C and 400°C and $P_f = 35$ MPa approach those for supercritical water. Solubility of solutes and reaction rates in the supercritical state are significantly elevated (Weingärtner & Franck, 2005) and thus may impact intergranular pressure solution. Therefore, when the temperature exceeds the critical point between 300 and 400°C, the density of the water will change drastically (Sakuma & Ichiki, 2016) and may promote an elevated rate of pressure solution of feldspar in the range of 300°C–400°C–resulting in the velocity-dependent transition observed for the feldspar gouge. This, combined with the microstructural observation that localized shear zones disappear at $T = 300$°C. Moreover, the feldspar gouge also shows a transition in velocity dependence with the shear velocity stepping. For shearing rates switched between 0.61 μm/s and 0.061 μm/s, the frictional stability coefficients ($a-b$) of the gouge decrease with increasing temperature.

Our experimental results show that the frictional strength of feldspar gouge increases with increasing pore pressure at a constant temperature and exhibits slightly velocity-weakening behavior over the range of our experimental pore pressures (Figure 7d). By averaging the ($a-b$) values over all shear velocity steps in each experiment and through linear fitting, we note that the mean magnitude of ($a-b$) increases nearly linearly with increasing pore pressure (Figure S3b in Supporting Information S1)–consistent with the results of previous

10.1029/2023EA003492

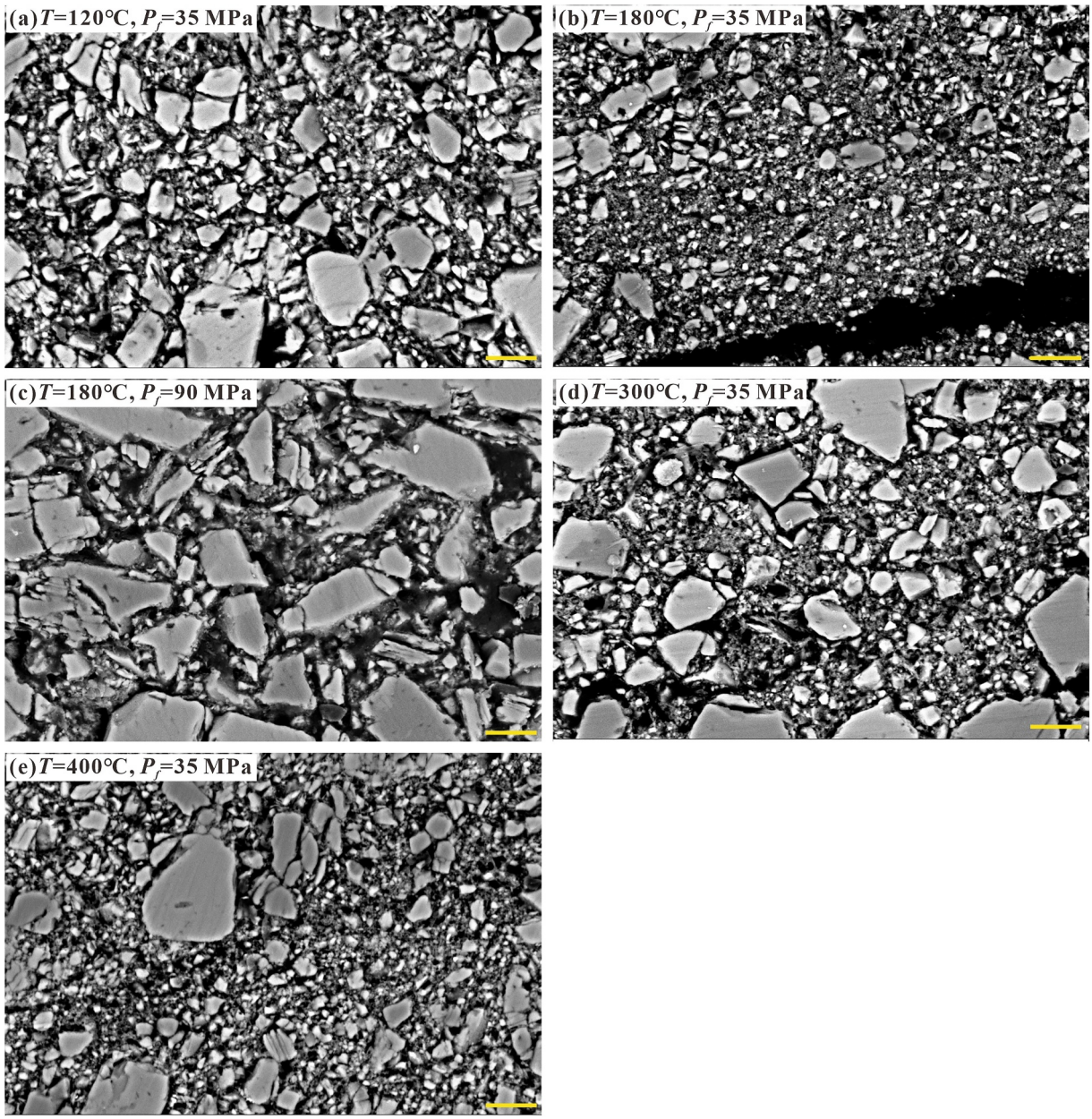

Figure 11. Particle fragmentation characteristics near the shear zone in the feldspar gouge after shearing. Among them, (b, c, e) exhibit velocity weakening behavior. Scale bar: 5 μm.

studies (Bedford et al., 2021; Xing et al., 2019). Previous systematic studies of quartz solubility have shown that quartz solubility increases with increasing pore pressure at the same temperature (Anderson & Burnham, 1965), and feldspar follows a similar pro-grade solubility trend (Li et al., 2018). Thus, the rate of feldspar pressure solution increases with increasing pore pressure. This is consistent with the above microphysical model in theory. That is, the pressure solution of feldspar becomes more vigorous and effective as a dissolution-diffusion process with an increase in pore pressure at the same experimental conditions—thus increasing the intergranular compaction velocity and decreasing porosity. As the intergranular contact area increases, the gouge frictional strength increases, and the average value of $(a-b)$ also slightly increases. The intergranular compactive velocity is approximately equivalent to the expansive velocity over our range of experimental pore pressures. However, the compactive velocity will exceed the expansive velocity at elevated pore pressures (>90 MPa), and the velocity dependence of the feldspar gouge may transition from velocity-weakening to velocity-strengthening (Verberne

10.1029/2023EA003492

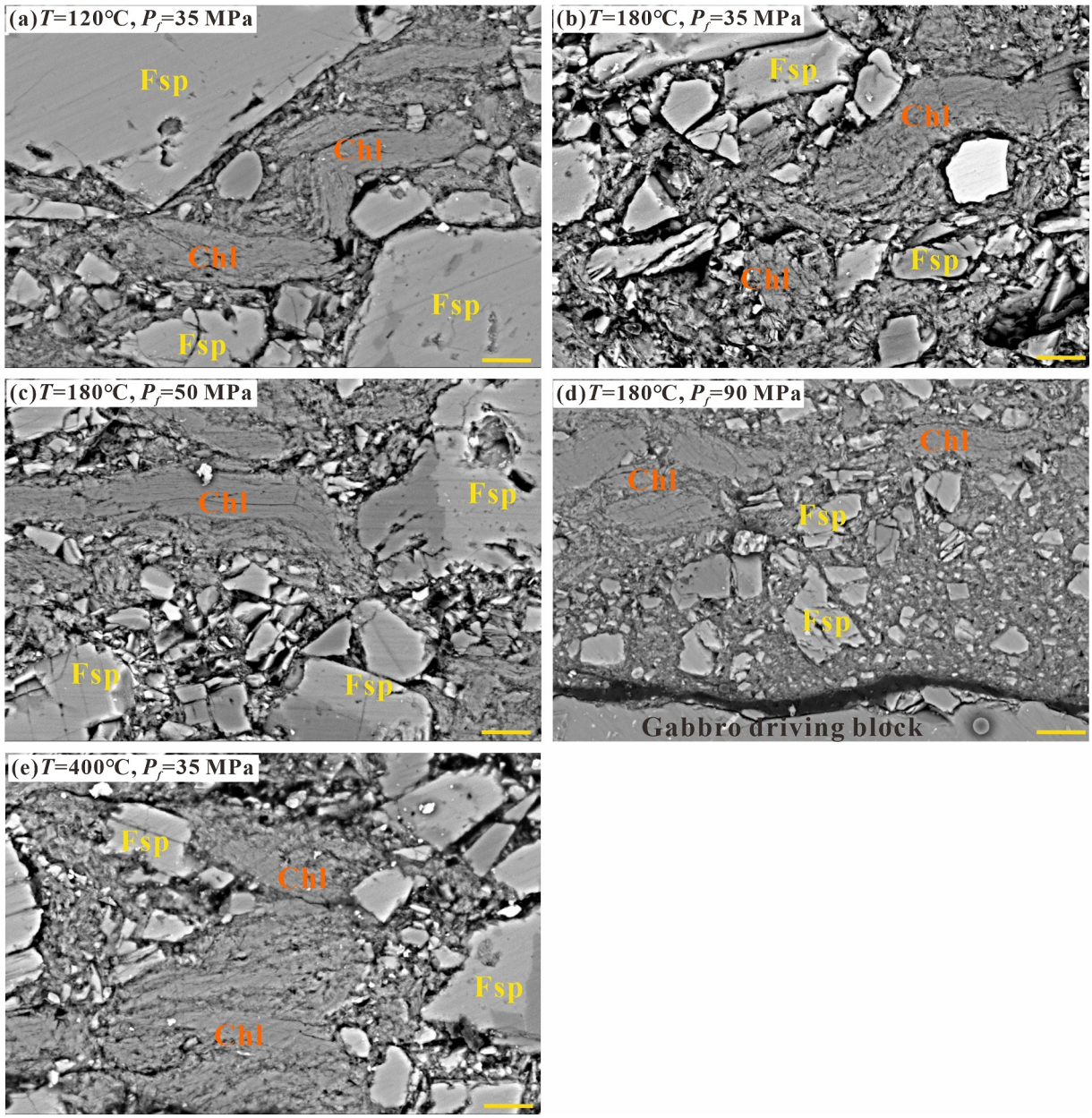

Figure 12. Particle fragmentation characteristics near the shear zone in the mixed feldspar-chlorite gouge after shearing. Among them, only (a) exhibits velocity-weakening behavior. Minerals: Fsp = Feldspar, Chl = chlorite. Scale bar: 5 μm.

et al., 2020). Moreover, the fabrics of the gouge samples differ characteristically for the various gouge frictional responses (velocity-strengthening vs. velocity-weakening) as apparent in the microstructures. Among them, grain size reduction in a localized shear zone appears to control the velocity-weakening behavior, and instability (Casas et al., 2023; Zhang & He, 2016). However, our experimental results show that the feldspar gouge exhibits velocity-weakening behavior at $P_f = 90$ MPa, with few distinct *R1* shear zones observed in the microstructures, rather, exhibiting regular shear fragmentation. The deformation of the gouge is dominated by rolling at high pore pressure and low effective stresses, and thus brittle rupture processes may be masked by the disappearance of localized shear zones in the gouge. This seems to explain why the feldspar gouge exhibits velocity-weakening behavior at high pore pressure, but with no obvious local shear zones observed in the microstructure.

4.2. Influence of Mineral Composition on Fault Friction

Fault sliding may transition from strengthen to weaken over long fluid-injection timescales at elevated temperatures, due to secondary mineral precipitation of hydrothermal alteration (Jeppson et al., 2023). Chlorite has a low coefficient of friction ($\mu = 0.25$–0.30) over our range of experimental temperature (≤400°C) and does not change significantly with temperature (Okamoto et al., 2019, 2020). Thus, the frictional coefficients of the feldspar-chlorite mixed gouge were significantly lower than those of the feldspar gouge and there is no clear evolution of the frictional coefficient of the mixed gouge with increasing temperature (Figure 7a). The frictional strengths of the feldspar-chlorite mixed gouges increase with increasing pore pressure. Moreover, the frictional strength of the feldspar gouge varies consistently for both contents at different temperatures and pore pressures. Our results show that chlorite as a low frictional strength altered mineral (An et al., 2021; Ikari et al., 2009; Okamoto et al., 2020) reduces only the overall frictional strength of the mixed gouges in our experiments, and not the style of deformation. That is, the presence of weak minerals in the mixed gouges (sheet silicates and strong minerals) reduces the frictional strength of the mixtures without changing the trend in frictional strength with increasing temperature and pore pressure, which is consistent with previous studies (Lu & He, 2018; Okamoto et al., 2020). The velocity dependence of the mixed gouges over the range of experimental temperatures reveals that the mixed gouges exhibit slight velocity-weakening ($T = 120$°C) and velocity-strengthening behavior ($T > 120$°C) and that the value of the velocity dependence parameter ($a-b$) increases with increasing temperature.

Our results indicate that the effect of different pore pressures on the frictional properties of feldspar-chlorite mixed gouges is similar to that of temperature. The frictional strength of the mixed gouges is significantly lower than that of the feldspar gouge and increases with increasing pore pressure. There is a consistent trend of frictional strength of gouges with pore pressure for the two feldspar contents (1:0 and 1:1). The feldspar-chlorite mixed gouges show velocity-strengthening behavior at our experimental pore pressure. There is a slight positive correlation between the values of velocity dependence parameter ($a-b$) and pore pressure in the mixed gouge at $T = 180$°C and $P_f = 35$ MPa (Figure 7d and Figure S3b in Supporting Information S1). The frictional stability of the mixed gouges is significantly enhanced compared to the feldspar gouge due to the presence of chlorite. Combining with the observations of microstructural characteristics of the deformed samples, we find that the *R1* shear becomes less obvious with increasing pore pressure at $P_f = 50-90$ MPa. The stability of the feldspar gouge increases with an increase in pore pressure. Moreover, compared with the frictional stability of chlorite (An et al., 2021; Ikari et al., 2009), albite (Masuda et al., 2019), plagioclase (He et al., 2013) and mixtures of quartz and clay minerals (Tembe et al., 2010) from previous experiments, the presence of feldspar minerals reduces the frictional stability of the mixed gouges over the range of our experimental temperatures, pore pressures and clay contents (Table S2 and Figure S3 in Supporting Information S1).

4.3. Implication for Injection-Induced Seismicity

Our experimental results are of significance for understanding the mitigation of induced seismicity under different hydrothermal conditions of granitic EGS reservoirs. EGS requires the injection of cold fluids (typically water) into the subsurface which typically results in a significant increase in pore pressure and a reduction in effective stress. Fluid transport relies on a connected network of natural and artificial fractures. Unexpectedly, large amounts of fluid may access undetected critically stressed faults (Grigoli et al., 2018), with alteration minerals conditioning the strength and stability of such faults (An et al., 2021; Zhang, Hu, et al., 2024). In high-temperature fractured reservoirs, the enhanced artificial circulation fluid volume will further accelerate the consumption of feldspar and the production of chlorite. This effect will lead to a decrease in the strength of exposed faults, as confirmed by laboratory friction experiments and microstructural observations (An et al., 2021; Fagereng & Ikari, 2020). Our experimental results show that the feldspar gouge presents slightly velocity-weakening behavior at $T = 180$°C and 400°C. This indicates that feldspar-rich faults may undergo unstable sliding as the depth of the modified reservoir increases. The feldspar/chlorite mixed gouges may promote stable sliding of faults, which implies that feldspar chloritization in EGS reservoirs of granite rock is a process with dynamic competitive effects. Chloritization in granite EGS reservoirs can influence the stability of faults although the influence on different minerals that are altered may be complex (Schmidt et al., 2018). In our experiments, we note feldspar chloritization as one of the sources of chlorite in granite EGS reservoirs–that if present–has an influential role in the unstable sliding of faults. Over the range of temperatures and pressures in our experiments, the result indicates that temperature alone may not be the major determinant of seismicity in granitic EGS reservoirs and emphasize the unique role of injection-fluid pressures. Meanwhile, the in-situ high temperature of the hydrothermal systems

may promote the fluid-assisted processes and thus modulating the stress states in reservoir scale (Chen et al., 2015; den Hartog et al., 2012; Martínez-Garzón et al., 2014; Westaway & Burnside, 2019). Thus, the co-moderating interaction of temperature and pore pressure may be important in triggering earthquakes in feldspar-rich EGS reservoirs.

Additionally, other influential factors in the triggering of injection-induced earthquakes in EGS reservoirs cannot be neglected, such as in situ driving slip rates. Our experiments show that feldspar-rich faults slide more unsteadily with decreasing shearing rate. Feldspar gouge generally exhibits velocity weakening behavior at shearing velocities of ~0.61 μm/s and ~0.061 μm/s at $T > 120$°C (Figures 8a and 8b), which suggests that unstable sliding of the fault occurs at low rates of shear sliding and thus may induce seismicity (Chen et al., 2015). Moreover, the driving slip rates in the laboratory are much higher than those in the natural faults (Chen et al., 2015). Thus, lower tectonic driving velocities may further reduce frictional stability, resulting in smaller and more negative values of ($a-b$) and then leading to unstable sliding of the faults (Ikari & Kopf, 2017). Further experimental studies are needed to analyze the effects of different mineral contents and shear velocity on fault stability. Our study has implications for natural faults rich in feldspar that may undergo feldspar-chloritization processes and are present at elevated temperatures and pressures in the subsurface.

5. Conclusions

Based on the hydrothermal conditions at the depth of the granitic EGS reservoir, we conducted shear experiments to explore the frictional stability of simulated feldspar (K-feldspar and albite) gouge and feldspar-chlorite mixed gouge. Meanwhile, the effects of different temperatures and pore pressures on fault sliding were analyzed. The experimental results show that the frictional strength of chlorite-rich mixed gouges is lower than that of feldspar gouges. The frictional stability of gouge is enhanced with the addition of chlorite in the mixed gouges, which suggests that the content of clay minerals in the gouge may be one of the controlling factors for the frictional behavior of the fault. Additionally, the feldspar gouge exhibits slightly velocity-weakening behavior and the average values of ($a–b$) slightly increase with increasing pore pressure under hydrothermal conditions. Combined with the analysis of the effects of temperature and pore pressure, we hypothesize that fluid injection operations within the depth range of the EGS modification may promote unstable sliding of potentially feldspar-rich faults, which suggests that feldspar-rich faults may be reactivated in granitic EGS reservoirs. Hence, the presence of feldspar gouge and feldspar chloritization sequences and the range of injection pressures need to be considered in the development of EGS to minimize the risk of injection-induced seismicity.

Data Availability Statement

The experimental data presented in this study are available at Hu et al. (2023).

Acknowledgments
The research was funded by National Natural Science Foundation of China (42177175), Central Public-interest Scientific Institution Basal Research Fund (DZLXJK202204), and China Geological Survey (DD20190138, DD20221660). We thank Prof. Changrong He for useful discussions of the raw test data. We appreciate the assistance of Wenming Yao and Xi Ma in running the original experiments. DE gratefully acknowledges support from the G. Albert Shoemaker endowment. We appreciate the helpful and constructive comments from Editor Kristy Tiampo and the three anonymous reviewers, which have greatly improved the quality of this manuscript.

References

An, M., Zhang, F., Chen, Z., Elsworth, D., & Zhang, L. (2020). Temperature and fluid pressurization effects on frictional stability of shale faults reactivated by hydraulic fracturing in the Changning block, southwest China. *Journal of Geophysical Research: Solid Earth*, *125*(8), e2020JB019584. https://doi.org/10.1029/2020JB019584

An, M., Zhang, F., Min, K. B., Elsworth, D., Marone, C., & He, C. (2021). The potential for low-grade metamorphism to facilitate fault instability in a geothermal reservoir. *Geophysical Research Letters*, *48*(11). https://doi.org/10.1029/2021GL093552

Anderson, G. M., & Burnham, C. W. (1965). The solubility of quartz in super-critical water. *American Journal of Science*, *263*(6), 494–511. https://doi.org/10.2475/ajs.263.6.494

Andrés, S., Santillán, D., Mosquera, J. C., & Cueto- Felgueroso, L. (2019). Delayed weakening and reactivation of rate- and- state faults driven by pressure changes due to fluid injection. *Journal of Geophysical Research: Solid Earth*, *124*(11), 11917–11937. https://doi.org/10.1029/2019JB018109

Bao, X., & Eaton, D. W. (2016). Fault activation by hydraulic fracturing in western Canada. *Science*, *354*(6318), 1406–1409. https://doi.org/10.1126/science.aag2583

Bedford, J. D., & Faulkner, D. R. (2021). The role of grain size and effective normal stress on localization and the frictional stability of simulated quartz gouge. *Geophysical Research Letters*, *48*(7), e2020GL092023. https://doi.org/10.1029/2020GL092023

Bedford, J. D., Faulkner, D. R., Allen, M. J., & Hirose, T. (2021). The stabilizing effect of high pore-fluid pressure along subduction megathrust faults: Evidence from friction experiments on accretionary sediments from the Nankai Trough. *Earth and Planetary Science Letters*, *574*, 117161. https://doi.org/10.1016/j.epsl.2021.117161

Bedford, J. D., Faulkner, D. R., & Lapusta, N. (2022). Fault rock heterogeneity can produce fault weakness and reduce fault stability. *Nature Communications*, *13*(1), 326. https://doi.org/10.1038/s41467-022-27998-2

Blanpied, M. L., Lockner, D. A., & Byerlee, J. D. (1991). Fault stability inferred from granite sliding experiments at hydrothermal conditions. *Geophysical Research Letters*, *18*(4), 609–612. https://doi.org/10.1029/91GL00469

Blanpied, M. L., Lockner, D. A., & Byerlee, J. D. (1995). Frictional slip of granite at hydrothermal conditions. *Journal of Geophysical Research*, *100*(B7), 13045–13064. https://doi.org/10.1029/95JB00862

Brown, K. M., Kopf, A., Underwood, M. B., & Weinberger, J. L. (2003). Compositional and fluid pressure controls on the state of stress on the Nankai subduction thrust: A weak plate boundary. *Earth and Planetary Science Letters*, *214*(3–4), 589–603. https://doi.org/10.1016/S0012-821X(03)00388-1

Casas, N., Mollon, G., & Daouadji, A. (2023). Influence of grain-scale properties on localization patterns and slip weakening within dense granular fault gouges. *Journal of Geophysical Research: Solid Earth*, *128*(3), e2022JB025666. https://doi.org/10.1029/2022JB025666

Chen, J., & Spiers, C. J. (2016). Rate and state frictional and healing behavior of carbonate fault gouge explained using microphysical model. *Journal of Geophysical Research: Solid Earth*, *121*(12), 8642–8665. https://doi.org/10.1002/2016JB013470

Chen, J., Verberne, B. A., & Niemeijer, A. R. (2020). Flow-to-friction transition in simulated calcite gouge: Experiments and microphysical modeling. *Journal of Geophysical Research: Solid Earth*, *125*(11). https://doi.org/10.1029/2020JB019970

Chen, J., Verberne, B. A., & Spiers, C. J. (2015). Effects of healing on the seismogenic potential of carbonate fault rocks: Experiments on samples from the Longmen Shan Fault, Sichuan, China. *Journal of Geophysical Research: Solid Earth*, *120*(8), 5479–5506. https://doi.org/10.1002/2015JB012051

Chester, F. M., & Higgs, N. G. (1992). Multimechanism friction constitutive model for ultrafine quartz gouge at hypocentral conditions. *Journal of Geophysical Research. Part B: Solid Earth*, *97*(B2), 1859–1870. https://doi.org/10.1029/91JB02349

den Hartog, S. A., Peach, C. J., de Winter, D. M., Spiers, C. J., & Shimamoto, T. (2012). Frictional properties of megathrust fault gouges at low sliding velocities: New data on effects o-f normal stress and temperature. *Journal of Structural Geology*, *38*, 156–171. https://doi.org/10.1016/j.jsg.2011.12.001

Dieterich, J. H. (1978). Preseismic fault slip and earthquake prediction. *Journal of Geophysical Research*, *83*(B8), 3940–3948. https://doi.org/10.1029/JB083iB08p03940

Elders, W. A., Hoagland, J. R., Mcdowell, S. D., & Cobo, J. (1979). Hydrothermal mineral zones in the geothermal reservoir of Cerro Prieto. *Geothermics*, *8*(3–4), 201–209. https://doi.org/10.1016/0375-6505(79)90042-7

Ellsworth, W. L. (2013). Injection-induced earthquakes. *Science*, *341*(6142), 1225942. https://doi.org/10.1126/science.1225942

Eyre, T. S., Eaton, D. W., Garagash, D. I., Zecevic, M., Venieri, M., Weir, R., & Lawton, D. C. (2019). The role of aseismic slip in hydraulic fracturing-induced seismicity. *Science Advances*, *5*(8), 1–11. https://doi.org/10.1126/sciadv.aav7172

Fagereng, Å., & Ikari, M. J. (2020). Low-temperature frictional characteristics of chlorite-epidote-amphibole assemblages: Implications for strength and seismic style of retrograde fault zones. *Journal of Geophysical Research: Solid Earth*, *125*(4), e2020JB019487. https://doi.org/10.1029/2020JB019487

Faulkner, D. R., Sanchez-Roa, C., Boulton, C., & den Hartog, S. A. M. (2018). Pore fluid pressure development in compacting fault gouge in theory, experiments, and nature. *Journal of Geophysical Research: Solid Earth*, *123*(1), 226–241. https://doi.org/10.1002/2017JB015130

Grigoli, F., Cesca, S., Rinaldi, A. P., Manconi, A., López-Comino, J. A., Clinton, J. F., et al. (2018). The November 2017 Mw5.5 Pohang earthquake: A possible case of induced seismicity in South Korea. *Science*, *360*(6392), 1003–1006. https://doi.org/10.1126/science.aat2010

Gu, J. C., Rice, J. R., Ruina, A. L., & Tse, S. T. (1984). Slip motion and stability of a single degree of freedom elastic system with rate and state dependent friction. *Journal of the Mechanics and Physics of Solids*, *32*(3), 167–196. https://doi.org/10.1016/0022-5096(84)90007-3

He, C., Luo, L., Hao, Q. M., & Zhou, Y. (2013). Velocity-weakening behavior of plagioclase and pyroxene gouges and stabilizing effect of small amounts of quartz under hydrothermal conditions. *Journal of Geophysical Research: Solid Earth*, *118*(7), 3408–3430. https://doi.org/10.1002/jgrb.50280

He, C., Yao, W., Wang, Z., & Zhou, Y. (2006). Strength and stability of frictional sliding of gabbro gouge at elevated temperatures. *Tectonophysics*, *427*(1–4), 217–229. https://doi.org/10.1016/j.tecto.2006.05.023

Hu, Z., Zhang, C., Zhang, L., Elsworth, D., Gan, Q., Lei, H., et al. (2023). Frictional properties of feldspar-chlorite altered gouges and implications for Fault Reactivation in hydrothermal systems [Dataset]. *Dryad*. https://doi.org/10.5061/dryad.4b8gthtkc

Hubbert, M. K., & Rubey, W. W. (1959). Role of fluid Pressure in mechanics of overthrust faulting. *Geological Society of America Bulletin*, *70*(2), 115–166. https://doi.org/10.1130/0016-7606(1959)70[115:ROFPIM]2.0.CO;2

Hunfeld, L. B., Niemeijer, A. R., & Spiers, C. J. (2017). Frictional properties of simulated fault gouges from the seismogenic Groningen gas field under in situ P–T -chemical conditions. *Journal of Geophysical Research: Solid Earth*, *122*(11), 8969–8989. https://doi.org/10.1002/2017JB014876

Ikari, M. J., & Kopf, A. J. (2017). Seismic potential of weak, near-surface faults revealed at plate tectonic slip rates. *Science Advances*, *3*(11), e1701269. https://doi.org/10.1126/sciadv.1701269

Ikari, M. J., Marone, C., & Saffer, D. M. (2011). On the relation between fault strength and frictional stability. *Geology*, *39*(1), 83–86. https://doi.org/10.1130/G31416.1

Ikari, M. J., Saffer, D. M., & Marone, C. (2009). Frictional and hydrologic properties of clay-rich fault gouge. *Journal of Geophysical Research*, *114*(B5). https://doi.org/10.1029/2008JB006089

Jeppson, T. N., Lockner, D. A., Beeler, N. M., & Moore, D. E. (2023). Time-dependent weakening of granite at hydrothermal conditions. *Geophysical Research Letters*, *50*(21), e2023GL105517. https://doi.org/10.1029/2023GL105517

Li, T., Li, H., & Xu, L. (2018). An experimental study of interaction between pure water and alkaline feldspar at high temperatures and pressures. *Acta Geochimica*, *37*(1), 60–67. https://doi.org/10.1007/s11631-017-0208-9

Lockner, D. A., Summers, R., & Byerlee, J. D. (1986). Effects of temperature and sliding rate on frictional strength of granite. *Pure and Applied Geophysics*, *124*(3), 445–469. https://doi.org/10.1007/BF00877211

Logan, J. M., Dengo, C. A., Higgs, N. G., & Wang, Z. Z. (1992). Fabrics of experimental fault zones: Their development and relationship to mechanical behavior. In *International geophysics* (Vol. 51, pp. 33–67). Academic Press. https://doi.org/10.1016/S0074-6142(08)62814-4

Lu, Z., & He, C. (2018). Friction of foliated fault gouge with a biotite interlayer at hydrothermal conditions. *Tectonophysics*, *740*, 72–92. https://doi.org/10.1016/j.tecto.2018.05.003

Lucie, M. (2016). Quantifying hydrothermal alteration with normative minerals and other chemical tools at the Beattie Syenite, Abitibi greenstone belt, Canada. *Eochemistry-Exploration Environment Analysis*, *16*(3–4), 233–244. https://doi.org/10.1144/geochem2016-410

Majer, E. L., Baria, R., Stark, M., Oates, S., Bommer, J., Smith, B., & Asanuma, H. (2007). Induced seismicity associated with enhanced geothermal systems. *Geothermics*, *36*(3), 185–222. https://doi.org/10.1016/j.geothermics.2007.03.003

Marone, C. (1998). Laboratory-derived friction laws and their application to seismic faulting. *Annual Review of Earth and Planetary Sciences*, *26*(1), 643–696. https://doi.org/10.1146/annurev.earth.26.1.643

Martínez-Garzón, P., Kwiatek, G., Sone, H., Bohnhoff, M., Dresen, G., & Hartline, C. (2014). Spatiotemporal changes, faulting regimes, and source parameters of induced seismicity: A case study from the Geysers geothermal field. *Journal of Geophysical Research: Solid Earth*, *119*(11), 8378–8396. https://doi.org/10.1002/2014JB011385

Masuda, K. (2020). Frictional properties of anorthite (feldspar): Implications for the lower boundary of the seismogenic zone. *Earth Planets and Space*, *72*(1), 1–6. https://doi.org/10.1186/s40623-020-01271-6

Masuda, K., Arai, T., & Takahashi, M. (2019). Effects of frictional properties of quartz and feldspar in the crust on the depth extent of the seismogenic zone. *Progress in Earth and Planetary Science*, *6*(1), 1–8. https://doi.org/10.1186/s40645-019-0299-5

Maxim, F., Karalis, K., Boillat, P., Banuti, D. T., Marquez Damian, J. I., Niceno, B., & Ludwig, C. (2021). Thermodynamics and dynamics of supercritical water pseudo-boiling. *Advanced Science*, *8*(3). https://doi.org/10.1002/advs.202002312

Morrow, C. A., Moore, D. E., & Lockner, D. A. (2000). The effect of mineral bond strength and adsorbed water on fault gouge frictional strength. *Geophysical Research Letters*, *27*(6), 815–818. https://doi.org/10.1029/1999GL008401

Niemeijer, A. R., & Spiers, C. J. (2007). A microphysical model for strong velocity weakening in phyllosilicate-bearing fault gouges. *Journal of Geophysical Research*, *112*(B10), B10405. https://doi.org/10.1029/2007JB005008

Okamoto, A. S., Niemeijer, A. R., Takeshita, T., Verberne, B. A., & Spiers, C. J. (2020). Frictional properties of actinolite-chlorite gouge at hydrothermal conditions. *Tectonophysics*, *779*, 228377. https://doi.org/10.1016/j.tecto.2020.228377

Okamoto, A. S., Verberne, B. A., Niemeijer, A. R., Takahashi, M., Shimizu, I., Ueda, T., & Spiers, C. J. (2019). Frictional properties of simulated chlorite gouge at hydrothermal conditions: Implications for subduction megathrusts. *Journal of Geophysical Research: Solid Earth*, *124*(5), 4545–4565. https://doi.org/10.1029/2018JB017205

Ruina, A. (1983). Slip instability and state variable friction laws. *Journal of Geophysical Research*, *88*(B12), 10359–10370. https://doi.org/10.1029/JB088iB12p10359

Sakuma, H., & Ichiki, M. (2016). Density and isothermal compressibility of supercritical H2O–NaCl fluid: Molecular dynamics study from 673 to 2000 K, 0.2 to 2 GP a, and 0 to 22 wt% NaCl concentrations. *Geofluids*, *16*(1), 89–102. https://doi.org/10.1111/gfl.12138

Schiffman, P., & Fridleifsson, G. O. (1991). The smectite-chlorite transition in drillhole NJ-15, Nesjavellir geothermal field, Iceland: XRD, BSE and electron microprobe investigations. *Journal of Metamorphic Geology*, *9*(6), 679–696. https://doi.org/10.1111/j.1525-1314.1991.tb00558.x

Schmidt, R. B., Bucher, K., & Stober, I. (2018). Experiments on granite alteration under geothermal reservoir conditions and the initiation of fracture evolution. *European Journal of Mineralogy*, *30*(5), 899–916. https://doi.org/10.1127/ejm/2018/0030-2771

Scholz, C. (1998). Earthquakes and friction laws. *Nature*, *391*(6662), 37–42. https://doi.org/10.1038/34097

Scholz, C. (2019). *The mechanics of earthquakes and faulting* (3rd ed.). Cambridge University Press. https://doi.org/10.1017/9781316681473

Schultz, R., Skoumal, R. J., Brudzinski, M. R., Eaton, D., Baptie, B., & Ellsworth, W. (2020). Hydraulic fracturing-induced seismicity. *Reviews of Geophysics*, *58*(3), e2019RG000695. https://doi.org/10.1029/2019RG000695

Shimamoto, T., & Logan, J. M. (1981). Effects of simulated clay gouges on the sliding behavior of Tennessee sandstone. *Tectonophysics*, *75*(3–4), 243–255. https://doi.org/10.1016/0040-1951(81)90276-6

Tembe, S., Lockner, D. A., & Wong, T.-F. (2010). Effect of clay content and mineralogy on frictional sliding behavior of simulated gouges: Binary and ternary mixtures of quartz, illite, and montmorillonite. *Journal of Geophysical Research*, *115*(B3), B03416. https://doi.org/10.1029/2009JB006383

van der Elst, N. J., Savage, H. M., Keranen, K. M., & Abers, G. A. (2013). Enhanced remote earthquake triggering at fluid- injection sites in the midwestern United States. *Science*, *341*(6142), 164–167. https://doi.org/10.1126/science.1238948

Verberne, B. A., van den Ende, M. P., Chen, J., Niemeijer, A. R., & Spiers, C. J. (2020). The physics of fault friction: Insights from experiments on simulated gouges at low shearing velocities. *Solid Earth Discussions*, *2020*(6), 1–37. https://doi.org/10.5194/se-11-2075-2020

Weingärtner, H., & Franck, E. U. (2005). Supercritical water as a solvent. *Angewandte Chemie International Edition*, *44*(18), 2672–2692. https://doi.org/10.1002/anie.200462468

Westaway, R., & Burnside, N. M. (2019). Fault "corrosion" by fluid injection: A potential cause of the November 2017 Mw 5.5 Korean earthquake. *Geofluids*, *2019*, 1–23. https://doi.org/10.1155/2019/1280721

Xing, T., Zhu, W., French, M., & Belzer, B. (2019). Stabilizing effect of high pore fluid pressure on slip behaviors of gouge-bearing faults. *Journal of Geophysical Research: Solid Earth*, *124*(9), 9526–9545. https://doi.org/10.1029/2019JB018002

Yuguchi, T., Matsuki, T., Izumino, Y., Sasao, E., & Nishiyama, T. (2021). Mass transfer associated with chloritization in the hydrothermal alteration process of granitic pluton. *American Mineralogist*, *106*(7), 1128–1142. https://doi.org/10.2138/am-2020-7353

Yuguchi, T., Sasao, E., Ishibashi, M., & Nishiyama, T. (2015). Hydrothermal chloritization processes from biotite in the Toki granite, Central Japan: Temporal variations of the compositions of hydrothermal fluids associated with chloritization. *American Mineralogist*, *100*(5–6), 1134–1152. https://doi.org/10.2138/am-2015-5126

Zhang, C., Fan, D., Elsworth, D., He, M., Zhao, X., Zhu, C., & Zhang, H. (2024). Mechanisms of stress-and fluid-pressure-driven fault reactivation in Gonghe granite: Implications for injection-induced earthquakes. *International Journal of Rock Mechanics and Mining Sciences*, *174*, 105642. https://doi.org/10.1016/j.ijrmms.2024.105642

Zhang, C., Hu, Z., Elsworth, D., Zhang, L., Zhang, H., Zhang, L., et al. (2024). Frictional stability of laumontite under hydrothermal conditions and implications for injection-induced seismicity in the Gonghe geothermal reservoir, northwest China. *Geophysical Research Letters*, *51*(10), e2023GL108103. https://doi.org/10.1029/2023GL108103

Zhang, F., Huang, R., An, M., Min, K. B., Elsworth, D., Hofmann, H., & Wang, X. (2022). Competing controls of effective stress variation and chloritization on friction and stability of faults in granite: Implications for seismicity triggered by fluid injection. *Journal of Geophysical Research: Solid Earth*, *127*(8). https://doi.org/10.1029/2022JB024310

Zhang, E., Wen, D., Wang, G., Yan, W. D., Wang, W. S., Ye, C. M., et al. (2022). The first power generation test of hot dry rock resources exploration and production demonstration project in the Gonghe Basin, Qinghai Province, China. *China Geology*, *5*(3), 372–382. https://doi.org/10.31035/cg2022038

Zhang, L., & He, C. (2016). Frictional properties of phyllosilicate-rich mylonite and conditions for the brittle-ductile transition. *Journal of Geophysical Research: Solid Earth*, *121*(4), 3017–3047. https://doi.org/10.1002/2015JB012489

Zhao, Y., Feng, B., Zhang, G., Shangguan, S., Qi, X., Li, X., et al. (2020). Study of the interaction between the granitic hot-dry rock (HDR) and different injection waters. *Acta Geologica Sinica*, *94*(07), 2115–2123. (in Chinese).